International Journal of Adhesion & Adhesives 31 (2011) 455–465

Contents lists available at ScienceDirect

International Journal of Adhesion & Adhesives

journal homepage: www.elsevier.com/locate/ijadhadh

Analysis of adhesive-bonded single-lap joint with an interfacial crack and a void

Alireza Chadegani, Romesh C. Batra *

Department of Engineering Science and Mechanics, Virginia Polytechnic Institute and State University, Blacksburg, VA 24061, USA

ARTICLE INFO

Article history:
Accepted 26 February 2011
Available online 9 March 2011

Keywords:
Adhesive-bonded joint
First-order shear deformation theory
Interfacial crack
Mode-mixity parameter
Strain energy release rate
Stress singularity
Void

ABSTRACT

We use the first-order shear deformation plate theory (FSDT) to analyze stresses in two layers bonded together with an adhesive as recommended by the ASTM D3165 standard, except that we also include a void within the adhesive. Depending upon the number of notches and voids, the specimen is divided into several regions. Assuming that a plane strain state of deformation prevails in the specimen, we write the balance of forces and moments for each section and impose the continuity of displacements, forces and moments at the interfaces between the adjoining sections. By taking the Laplace transform of the resulting ordinary differential equations we get a system of simultaneous linear algebraic equations that can be easily solved. The inverse transform of the solution of the algebraic equations provides stresses and displacements in the adhesive and the substrates, which are found to agree well with those obtained by the finite element method (FEM). It is also found that the order of the stress singularity at the corner of the free surface of the adhesive and the substrate, and the strain energy release rate computed from the solution of the problem with the FSDT agree well with those determined from the solution of the problem by the FEM. We note that the computational effort required to analyze the problem with the FSDT is considerably less than that needed to solve the problem by the FEM.

1. Introduction

Adhesive-bonded joints are increasingly being used in aerospace and automotive industries due to the ease with which they can be formed. Like other joints, e.g. bolted joints, one of the issues in adhesive-bonded joints is the prediction of failure mechanisms. Two major failure mechanisms widely reported in adhesive-bonded joints are interfacial and cohesive fractures [1–6]. The interfacial fracture refers to the separation of the adhesive from the substrate at the interface between the two possibly due to either the normal or the shear stress or their suitable combination exceeding the bond strength between the adhesive and the substrate. The cohesive failure refers to the failure of the adhesive at a point within the adhesive. Either defects at the adhesive/substrate interface or poor bonding between the two materials or cracks initiating at the site of the stress singularity may result in the interfacial failure.

An often used criterion for crack initiation is the critical strain energy release rate (SERR), i.e., a crack is assumed to initiate when the SERR reaches a material-dependent critical value. For an adhesive-bonded joint, the critical value of the SERR will depend upon the materials of the substrate and the adhesive. The order of stress singularity at the corner of the free surfaces of the substrate and the adhesive depends upon the elastic constants of the two materials generally through Dundurs' parameters [7]. One can ascertain the order of the stress singularity and stresses in the substrate and the adhesive by using the finite element method (FEM) but it is computationally very expensive since the FE mesh required to accurately compute the stress singularity needs to be extremely fine.

Under general loading the interfacial failure is a mixed-mode process that may include one or more of the three failure modes, namely, the crack opening mode I, the shearing mode II, and the tearing mode III. One thus needs to ascertain the effective SERR that incorporates all three failure modes.

Adhesively bonded joints have been studied, amongst others, by Goland and Reissner [8], Erdogan and Ratwani [9], and Hart-Smith [10]. There is enormous literature on the analysis of adhesive-bonded joints; we refer the reader to review papers by Kutscha [11], Kutscha and Hofer [12], Matthews et al. [13], Vinson [14], da Silva et al. [15], and Zhao et al. [16]. Tsai and Morton [17] compared results from a two-dimensional (2-D) geometrically nonlinear FE analysis with those from the analytical solutions. Yang and Pang [18] have analytically found stresses in adhesive-bonded single-lap joints. Huang et al. [19] and Yang et al. [20] have investigated the

* Correspondence to: 220 Norris Hall, Department of Engineering Science and Mechanics, Virginia Polytechnic Institute and State University, Blacksburg, VA 24061, USA. Tel.: +1 540 231 6051; fax: +1 540 2314574.

E-mail addresses: chadegan@vt.edu (A. Chadegani), rbatra@vt.edu (R.C. Batra).

0143-7496/$ - see front matter © 2011 Elsevier Ltd. All rights reserved.
doi:10.1016/j.ijadhadh.2011.02.006

Nomenclature

P	applied tensile load per unit width, N/m
u_x^i	x-displacement for ith substrate, mm
u_x^{oU}, u_x^{oL}	upper and lower substrates mid-plane x-displacement, mm
u_x^a	adhesive x-displacement, mm
ψ^{iU}, ψ^{iL}	upper and lower substrates angles of rotation of the transverse normal about the y_i-axis for ith substrate, rad
u_z^i	z-displacement field for ith substrate, mm
u_z^{oU}, u_z^{oL}	upper and lower substrates mid-plane z-displacement, mm
u_z^a	adhesive z-displacement, mm
ε_{xx}^i, ε_{zz}^i, γ_{xz}^i	strain components for ith substrate, mm/mm
ε_{xx}^a, ε_{zz}^a, γ_{xz}^a	adhesive strain components, mm/mm
N_x^i	axial force per unit width for ith substrate, N/m
M_y^i	bending moment per unit width for ith substrate, Nm/m
Q_z^i	transverse shear force per unit width for ith substrate, N/m
N_c, Q_c, M_c	equivalent crack-tip axial and transverse forces, and bending moment
k_s	shear correction factor
h^U, h^L	thickness of upper and lower substrates, mm
W	work done to open the crack, J
σ_{xz}^a	adhesive shear stress, Pa
σ_{zz}^a	adhesive normal stress, Pa
η	adhesive thickness, mm
a	initial crack length, mm
b	virtual crack extension length, mm
L_c	current crack length, mm
L_o	total overlap length without a crack and a void, mm
L_n	notch length of ASTM D3165 specimen, mm
L_v	void length, mm
G_{I}	mode I strain energy release rate, J/m^2
G_{II}	mode II strain energy release rate, J/m^2
G_T	total strain energy release rate, J/m^2
β	mode-mixity parameter
$\overline{\alpha}$, $\overline{\beta}$	Dundurs' parameters

problem by assuming the adhesive material to be elastic–plastic and considered asymmetry of the substrates and the effects of transverse shear deformation. Krueger [21] used the virtual crack closure technique (VCCT) and the FEM to determine the SERR. Davidson et al. [22] used the classical plate theory and the VCCT to find SERR for delamination of a composite plate. Kim and Kong [23] as well as Lou and Tong [24] have used the classical beam (or plate) theory to calculate the SERR. Yang et al. [25] included transverse shear deformation of the plate, studied behavior of single-lap joints with interfacial crack and calculated the SERR. A comparative study of the analytical models can be found in a review paper by da Silva et al. [26]. Other works that used the VCCT to determine the SERR include those of Wang et al. [27], Wei et al. [28], and Crocombe et al. [29]. Contour integrals to compute the SERR have been employed, amongst others, by Fernlund et al. [30], Chadegani et al. [31], and Chen et al. [32]. Yang et al. [25,33] studied the effect of an interfacial crack in adhesive-bonded joints with composite substrates. In these studies the adhesive-bonded joint is assumed to have no flaws and voids (or gaps).

The effects of flaws and voids in adhesive-bonded joints have been studied, amongst others, by Hart-Smith [34], Kan and Ratwani [35], and Rossettos and Zang [36]. They used a shear-lag model where the substrates support the axial load and the adhesive is deformed primarily in shear. It should be noted that this model is appropriate when the applied loads do not cause bending of the joint. Rossettos et al. [37] adopted a modified shear-lag model by Rossettos and Shishesaz [38] assuming a quadratic distribution of the axial displacement in the adhesive. Olia and Rossetos [39] presented an analytical solution for a simple lap-joint with a void considering the effect of bending in their formulation of the problem. Lang and Mallick [40] studied the effect of a void in a single-lap joint with spew fillets using the FEM. de Moura et al. [41] evaluated the influence of strip defects on the mechanical behavior of composite bonded joints using the FEM and including interfacial decohesion based on a mixed-mode damage initiation and growth law. You et al. [42] employed the FEM to investigate the effect of a void on the stress distribution in an adhesive-bonded double-lap joint.

Here we use the first-order shear deformation theory (FSDT) to analyze stresses and displacements in an adhesive-bonded joint with an interfacial crack and a void; the void represents a region where there is no adhesive present between the two substrates. We assume that both the adhesive and the substrates are made of linear elastic, isotropic, and homogeneous materials. It is shown that the FSDT provides good values of the order of stress singularity and the SERR. Since this method is computationally inexpensive it can be used to conduct parametric studies, and to select between various preliminary designs of joints. The selected few designs can be further analyzed and narrowed down by using the FEM. Of course, there is no substitute for experimentally insuring that the proposed designs will work in practice.

2. Formulation of the problem

We study plane strain infinitesimal deformations of an ASTM D3165 standard specimen [43] composed of four metallic substrate segments bonded by thin layers of adhesive as shown in Fig. 1. We use rectangular Cartesian coordinates to describe deformations of the upper substrates of thickness h^U and the lower substrates of thickness h^L joined by the adhesive layer of thickness η. The tensile load per unit width (the dimension

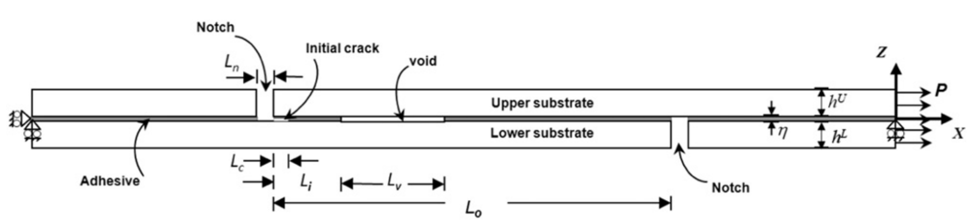

Fig. 1. ASTM D3165 geometry including an interfacial crack and a void.

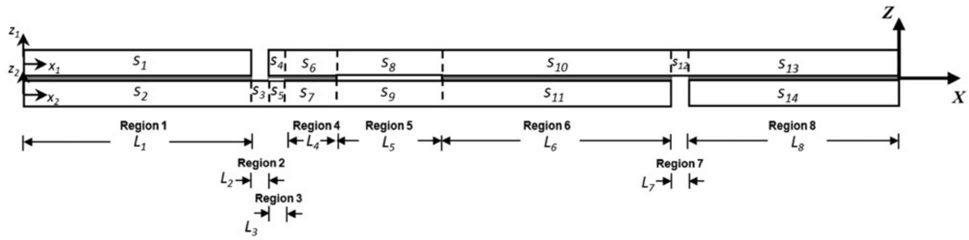

Fig. 2. Discretizaion of the specimen into subregions.

perpendicular to the plane of the paper), P, is applied along the x-axis to the right end of the single lap-joint specimen that is held fixed at the left end. Because of the notches present in the upper and the lower substrates the adhesive is mostly deformed in shear. We assume that during use an interfacial crack of length L_c has developed right after the first notch as shown in Fig. 1, and there is a void where no adhesive exists between the two substrates. The void could form either because the adhesive at the location of the void has evaporated or there was a manufacturing defect that went undetected. The location and the length of the void are varied to evaluate their effects on the performance of the lap-joint. A simplifying assumption is that prior to the application of the load P, the two substrates and the adhesive are stress free.

Assuming that the thickness h^U of the upper substrate, the thickness h^L of the lower substrate, and the thickness η of the adhesive are small as compared to their lengths and widths, we use the FSDT to describe deformations of the substrates and the adhesive. Starting from the left edge surface we divide the body into eight regions depicted in Fig. 2. Thus each substrate is divided into seven parts shown in Fig. 2. The number of regions into which the specimen is divided depends upon the number of notches, the number of initial cracks, and the number of voids present. For each region we write equations of equilibrium for the upper substrate, the adhesive, and the lower substrate.

2.1. Equations for a substrate

For each substrate S_i (i=1, 2,..., 14) we use local rectangular Cartesian coordinates (x_i,y_i,z_i) with the origin at the midpoint of the left edge of the substrate. In the FSDT displacements u_x and u_z in substrate S_i are approximated by

$$u_x(x_i,z_i) = u_x^o(x_i) + z_i\psi(x_i) \tag{1a}$$

$$u_z(x_i,z_i) = u_z^o(x_i) \tag{1b}$$

where the superscript "o" represents the quantity associated with the mid-plane and ψ is related to the rotation of the transverse normal about the y_i-axis. Eqs. (1a) and (1b) give the following expressions for the infinitesimal strains in substrate S_i

$$\varepsilon_{xx}^i = \frac{\partial u_x(x_i,z_i)}{\partial x_i} = \frac{du_x^o(x_i)}{dx_i} + z_i\frac{d\psi(x_i)}{dx_i} \tag{2a}$$

$$\varepsilon_{zz}^i = \frac{\partial u_z(x_i,z_i)}{\partial z_i} = 0 \tag{2b}$$

$$\gamma_{xz}^i = \frac{\partial u_z(x_i,z_i)}{\partial x_i} + \frac{\partial u_x(x_i,z_i)}{\partial z_i} = \frac{du_z^o(x_i)}{dx_i} + \psi(x_i) \tag{2c}$$

Assuming that the material of substrate S_i is linear elastic, stresses σ_{xx}^i, σ_{zz}^i, and $-\sigma_{xz}^i$ in S_i are given by

$$\sigma_{xx}^i = C_{11}^i\varepsilon_{xx}^i + C_{22}^i\varepsilon_{zz}^i \tag{3a}$$

$$\sigma_{zz}^i = C_{22}^i\varepsilon_{xx}^i + C_{33}^i\varepsilon_{zz}^i \tag{3b}$$

$$\sigma_{xz}^i = C_{44}^i\gamma_{xz}^i \tag{3c}$$

where C_{11}^i ,C_{22}^i , C_{33}^i , and C_{44}^i are elastic constants for the material of S_i. The resultant normal and shear forces N_x^i, Q_z^i, and the bending moment M_y^i per unit width of S_i are given by

$$N_x^i = \int \sigma_{xx}^i dz_i \tag{4a}$$

$$Q_z^i = k_s\int \sigma_{xz}^i dz_i \tag{4b}$$

$$M_y^i = \int z_i\sigma_{xx}^i dz_i \tag{4c}$$

where the integration is over the thickness of the substrate S_i and k_s is the shear correction factor.

2.2. Equations for the adhesive

We presume that the adhesive, if present between the upper and the lower substrates, is perfectly bonded to them. Furthermore, because of the small thickness η of the adhesive, the strain components at a point in the adhesive are approximated by

$$2\varepsilon_{xx}^{ai} = \frac{d}{dx_i}\left[u_x^{oU}(x_i) - \frac{h^U}{2}\psi^{iU}(x_i) + u_x^{oL}(x_i) + \frac{h^L}{2}\psi^{iL}(x_i)\right] \tag{5a}$$

$$\gamma_{xz}^{ai} = \frac{1}{\eta}\left[u_x^{oU}(x_i) - \frac{h^U}{2}\psi^{iU}(x_i) - u_x^{oL}(x_i) - \frac{h^L}{2}\psi^{iL}(x_i)\right] + \frac{1}{2}\left[\frac{du_z^{oU}(x_i)}{dx_i} + \frac{du_z^{oL}(x_i)}{dx_i}\right] \tag{5b}$$

$$\varepsilon_{zz}^{ai} = \frac{1}{\eta}\left[u_z^{oU}(x_i)\text{-}u_z^{oL}(x_i)\right] \tag{5c}$$

where superscripts U and L signify, respectively, quantities for the upper and the lower substrates, and the superscript "a" stands for the adhesive. It is known that the last term on the right hand side of Eq. (5b) has negligible effect, (see Ref. [39]), and the inclusion of this term often makes it hard to solve the problem. Since we use symbolic software, the retention of this term poses no difficulty, and mitigates the need to make one additional assumption.

Assuming that the adhesive material is linear elastic and isotropic, the axial stress σ_{xx} in the adhesive is negligible, the normal (peel) and the shear stresses in the adhesive are given by

$$\sigma_{zz}^{ai} = \overline{C}_{22}^a\varepsilon_{xx}^{ai} + \overline{C}_{33}^a\varepsilon_{zz}^{ai} \tag{6a}$$

$$\sigma_{xz}^{ai} = \overline{C}_{44}^a\gamma_{xz}^{ai} \tag{6b}$$

In view of the small thickness η of the adhesive, stresses and strains in it are taken to be functions of x_i only.

2.3. Equilibrium equations

In order to derive equilibrium equations we draw a free-body diagram of an element of length Δx_i of the substrate S_i; e.g., see Fig. 3.

The balance of forces and moments for the element of the upper substrate gives

$$\frac{dN_x^{iU}}{dx_i} = -\sigma_{xz}^{ai} \tag{7a}$$

$$\frac{dM_y^{iU}}{dx_i} = Q_z^{iU} + \frac{h^U}{2}\sigma_{xz}^{ai} \tag{7b}$$

$$\frac{dQ_z^{iU}}{dx_i} = \sigma_{zz}^{ai} \tag{7c}$$

We write similar equations for the lower substrate. Boundary conditions for the upper substrate are

$$N_x^{iU} = 0, Q_z^{iU} = 0, M_y^{iU} = 0, \quad \text{at a traction-free vertical surface} \tag{8a}$$

$$u_x^{oiU} = 0, u_z^{oiU} = 0, M_y^{iU} = 0, \quad \text{at the left edge of the specimen} \tag{8b}$$

$$N_x^{iU} = P/2, u_z^{ioU} = 0, M_y^{iU} = 0, \quad \text{at the right loaded vertical surface} \tag{8c}$$

$$\sigma_{xz}^{ai} = 0, \sigma_{zz}^{ai} = 0, \quad \text{at the traction-free bottom horizontal surface} \tag{8d}$$

We impose the following boundary conditions on edges of the lower substrate.

$$u_x^{oiL} = 0, Q_z^{iL} = 0, M_y^{iL} = 0, \quad \text{at the left edge of the specimen} \tag{9a}$$

$$N_x^{iL} = P/2, Q_z^{iL} = 0, M_y^{iL} = 0, \quad \text{at the right loaded vertical surface} \tag{9b}$$

Because of St. Venant's principle boundary conditions at the left edge of the specimen will have a little effect on the stress field in regions other than region 1.

The continuity conditions at the vertical interface between segments i and $i+1$ of the upper substrate are

$$N_x^{iU} = N_x^{(i+1)U}, Q_z^{iU} = Q_z^{(i+1)U}, M_y^{iU} = M_y^{(i+1)U} \tag{10a}$$

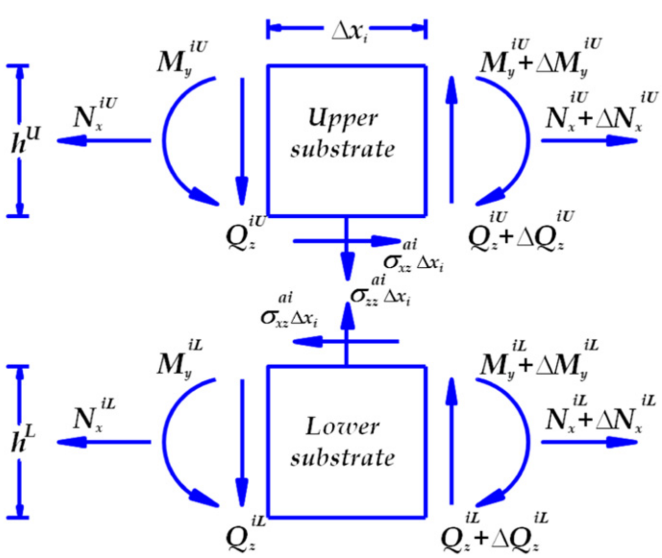

Fig. 3. Free-body diagram and sign convention.

$$u_x^{oiU} = u_x^{o(i+1)U}, u_z^{oiU} = u_z^{o(i+1)U}, \psi^{iU} = \psi^{(i+1)U} \tag{10b}$$

2.4. Solution technique

Combining Eqs. (1)–(7), we get second-order linear ordinary differential equations (ODEs) in terms of the generalized displacements u_x^{oiU}, ψ^{iU}, u_z^{oiU}, u_x^{oiL}, ψ^{iL} and u_z^{oiL}. Equilibrium equations for the lower and the upper substrates are related with each other through σ_{xz}^{ai} and σ_{zz}^{ai} appearing in Eqs. (7a)–(7c). Equations for segments i and $i+1$ are related through the equations expressing the continuity of surface tractions and displacements across the common vertical interface between them; e.g., see Eqs. (10a) and (10b).

For the specimen divided into 8 regions or 14 segments exhibited in Fig. 2, there will be 42 coupled second-order ODEs. Here we take the generalized displacements and their first-order derivatives with respect to x as unknowns. Thus we need to simultaneously solve 84 linear coupled first-order ODEs under the pertinent boundary conditions. We take the Laplace transform of these equations to get a system of linear algebraic equations, which are simultaneously solved for the unknowns. The inverse Laplace transform of these unknowns provides the generalized displacements from which stresses and strains are computed at any point of the specimen. The processes of taking the Laplace transform followed by taking the inverse Laplace transform are performed using the software MAPLE. Governing equations for each segment are solved first and then continuity and boundary conditions are used to evaluate the constants of integration.

3. Strain energy release rate calculation

In linear elastic fracture mechanics (LEFM) a crack is assumed to propagate when the SERR at the crack-tip attains a critical value. Here we assume that there exists a crack of length $L_c = a$ at

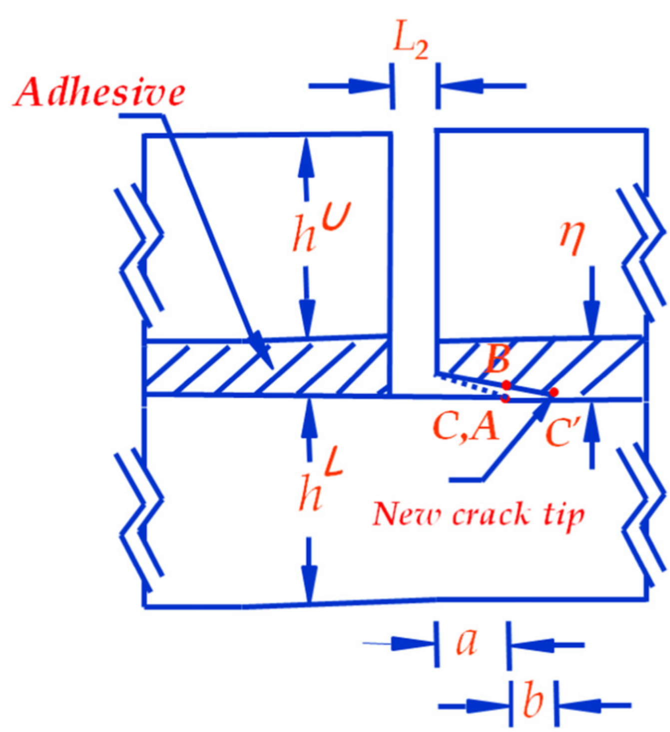

Fig. 4. ASTM D3165 specimen with an initial interfacial crack of length a, shown with dashed line, and a virtual crack extension of length b.

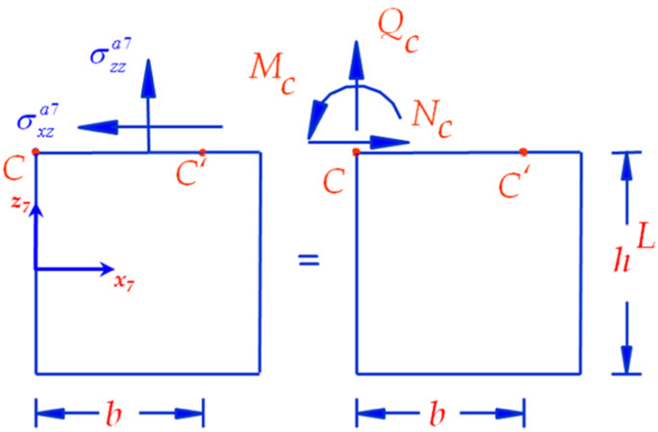

Fig. 5. Left: stresses on the top surface near the crack tip; right: equivalent forces and bending moment at the crack tip.

the adhesive/lower substrate interface immediately after the first notch and find the value of the SERR by two methods.

In order to compute the SERR by using the VCCT, we consider a virtual crack extension through length b from point C to point C'; e.g., see Fig. 4.

Prior to the crack extension, the overlap area between points C and C' adheres and there are in general non-zero normal and tangential tractions at the interface between the adhesive and the substrate.

These tractions on the interface CC', shown in Fig. 5, are related to the equivalent crack-tip forces and bending moment N_c, Q_c, and M_c as follows:

$$N_c = -\int_0^b \sigma_{xz}^{a7} dx_7 \tag{11a}$$

$$Q_c = \int_0^b \sigma_{zz}^{a7} dx_7 \tag{11b}$$

$$M_c = \int_0^b \sigma_{zz}^{a7} x_7 dx_7 \tag{11c}$$

Stresses σ_{xz}^{a7} and σ_{zz}^{a7} are obtained from the solution of the single-lap joint problem prior to the virtual extension of the crack-tip.

During the virtual extension of the crack-tip from point C to point C', the material point at C is assumed to split into two points A and B. In order to close the virtual crack, crack-tip forces and moments are applied at points A and B to move them back to their original locations. The work, W, required to close the virtual crack is given by

$$W = \tfrac{1}{2}[N_C(u_x^B - u_x^A) + M_C(\psi^B - \psi^A) + Q_C(u_z^B - u_z^A)] \tag{12}$$

where it has been tacitly assumed that N_c, M_c and Q_c vary linearly with $(u_x^B - u_x^A)$, $(\psi^B - \psi^A)$, and $(u_z^B - u_z^A)$, respectively. Values of u_x^A, u_x^B, etc. are found by solving the single-lap joint problem with the overlap length L_4 in Fig. 2 replaced by $L_4 - L_c$ and using the following relations:

$$u_x^B = u_x^{o4}|_{x_3 = L_3 - b} - \left(\frac{h^U}{2} + \eta\right)\psi^4|_{x_3 = L_3 - b} \tag{13a}$$

$$\psi^B = \psi^4|_{x_3 = L_3 - b} \tag{13b}$$

$$u_z^B = u_z^4|_{x_3 = L_3 - b} \tag{13c}$$

$$u_x^A = u_x^{o5}|_{x_3 = L_3 - b} + \frac{h^L}{2}\psi^5|_{x_3 = L_3 - b} \tag{13d}$$

$$\psi^A = \psi^5|_{x_3 = L_3 - b} \tag{13e}$$

$$u_z^A = u_z^5|_{x_3 = L_3 - b} \tag{13f}$$

We note that W also equals the energy released during the virtual extension of the crack through distance b. Thus for unit width of the specimen in the y-direction, the SERR is given by

$$G_T = G_I + G_{II} \tag{14a}$$

where

$$G_I = \frac{1}{2b}[M_C(\psi_B - \psi_A) + Q_C(u_z^B - u_z^A)] \tag{14b}$$

$$G_{II} = \frac{1}{2b}[N_C(u_x^B - u_x^A)] \tag{14c}$$

The mode-mixity parameter, β, is defined as

$$\beta = \tan^{-1}\left(\frac{G_{II}}{G_I}\right) \tag{15}$$

For pure mode I failure, $\beta = 0$, and $\beta = \pi/2$ for pure mode II failure.

4. Solution of the problem by the FEM

In order to ascertain the accuracy of results obtained by using the FSDT, we compare them with those obtained by using the commercial FE software ABAQUS [44]. The FE meshes for the two substrates and the adhesive are successively refined till the solution has converged as determined by comparing the computed order of singularity in the shear stress at the adhesive/substrate interface with its analytical value. The order of stress singularity depends upon Dundurs' parameters whose values depend upon the elastic constants of the two adjoining materials. The problem has been analyzed, amongst others, by Bogy and Wang [45]. Referring the reader to Qian and Akisanya [46] for details, we merely mention that equations of elastostatics for the two materials are solved in the neighborhood of point A shown in Fig. 6 with perfect bonding conditions imposed on the interface.

Denoting the shear moduli and Poisson's ratios of the two materials by subscripts 1 and 2, the order of stress singularity is

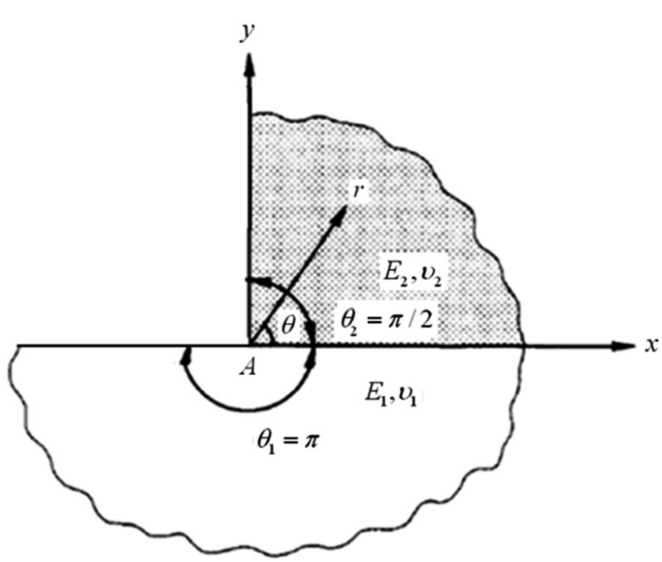

Fig. 6. Schematic sketch of the contact between two bodies.

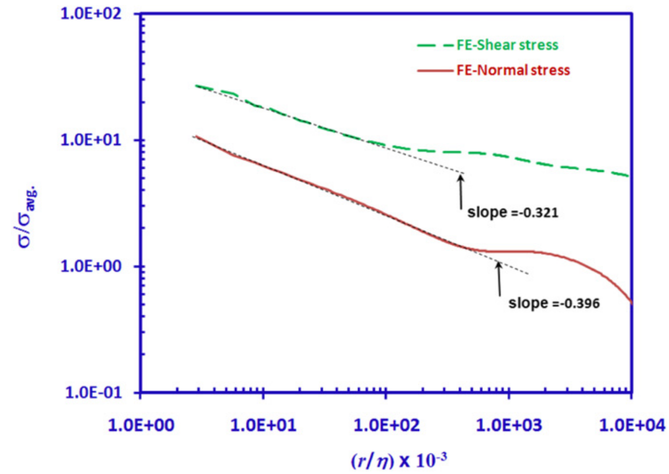

Fig. 7. On log–log scale, variation of the shear and the normal stresses with the distance from the corner.

given by [46]

$$\sigma_{ij}=\begin{cases} o(r^{-1+p}) & \text{if } p\in R \\ o[(r^{-1+\xi}\cos(\eta\log r)),(r^{-1+\xi}\sin(\eta\log r))] & \text{if } p\in C \\ o(\log r) & \text{if no zero occurs in } 0<\mathrm{Re}(p)<1 \\ & \text{but } \frac{dD}{dp}=0 \text{ at } p=1 \end{cases} \tag{16}$$

where $p=\xi+i\eta$ is a root of the following characteristic equation.

$$\begin{aligned} D(\overline{\alpha},\overline{\beta},\theta_1,\theta_2,p)=&[(\overline{\alpha}-\overline{\beta})^2p^2\sin(\theta_1)^2-(1-\overline{\beta})^2\sin(p\theta_1)^2] \\ &\times[(1+\overline{\beta})^2\sin(p\theta_2)^2-(\overline{\alpha}-\overline{\beta})^2p^2\sin(\theta_2)^2] \\ &+(\overline{\alpha}^2-1)\sin(p(\pi-\theta_2))^2[2(\overline{\alpha}-\overline{\beta})^2p^2\sin(\theta_2)^2 \\ &+2(1-\overline{\beta}^2)\sin(p\theta_1)\sin(p\theta_2)-(\overline{\alpha}^2-1)\sin(p(\pi-\theta_2))^2]=0 \end{aligned} \tag{17}$$

Angles θ_1 and θ_2 are defined in Fig. 6, and Dundurs' parameters $\overline{\alpha}$ and $\overline{\beta}$ are given by

$$\overline{\alpha}=\frac{G_1m_2-G_2m_1}{G_1m_2+G_2m_1} \tag{18a}$$

$$\overline{\beta}=\frac{G_1(m_2-2)-G_2(m_1-2)}{G_1m_2+G_2m_1} \tag{18b}$$

$$G_i=\frac{E_i}{2(1+\upsilon_i)},\quad m_i=\begin{cases}4(1-\upsilon_i) & \text{for plane strain} \\ \frac{4}{(1+\upsilon_i)} & \text{for plane stress}\end{cases}\quad i=1,2 \tag{18c}$$

As pointed out by Weissberg and Arcan [47] one needs a very fine FE mesh to accurately compute the stress singularity at the corner where free surfaces of the adhesive and the substrate intersect. The FE mesh was successively refined till a converged value of the order of stress singularity was achieved. In the neighborhood of the free edge the FE mesh was refined to three orders of magnitude more than that used for the rest of the region. For the aluminum substrate and the epoxy polymer adhesive, the computed value of the order of the singularity in the shear stress σ_{xz} at the interface equals 0.321 (see Fig. 7) which compares well with the analytical value of 0.322. We note that the computed order of the stress singularity in the normal stress is 0.396 whereas that in the analytical solution is 0.321. To calculate a converged value of the SERR, the FE mesh was refined so that the element height in the adhesive equaled $\eta/15$ while that in the substrate equaled $h^U/40$. The aspect ratio of a FE was taken to be 3.

5. Results for sample problems

In order to compute numerical results we consider substrates made of 2024-T3 aluminum [6] (E_{Al}=73 GPa, υ_{Al}=0.33) bonded together with a 0.1 mm thick FM-73 [6] epoxy adhesive (E_{adh}=1.64 GPa, υ_{adh}=0.35). We set the shear correction factor $k_s=5/6$, L_o=50.8 mm even though this value of k_s was proposed for thin monolithic plates/beams, the notch-size L_n=1.6 mm (see Fig. 1) and the lengths L_1 and L_8 of substrates outside the overlap (see Fig. 2) equal to 25.4 mm. The length, L_v, of the void is varied. Unless otherwise noted results are computed for $h^U=h^L$=1.6 mm.

We compute results for two configurations—one shown in Fig. 1 and the other in which there is no right notch; these two configurations are referred to as the double-notch and the single-notch, respectively.

For the single-notch and the double-notch specimens we have plotted in Figs. 8 and 9, respectively, the variation with the distance from the crack-tip of the shear and the normal stresses in the adhesive obtained from the solution of the problem by using the FSDT and the FEM. The two sets of results are very close to each other. At points away from the crack-tip the maximum difference between the normal and the shear stresses computed

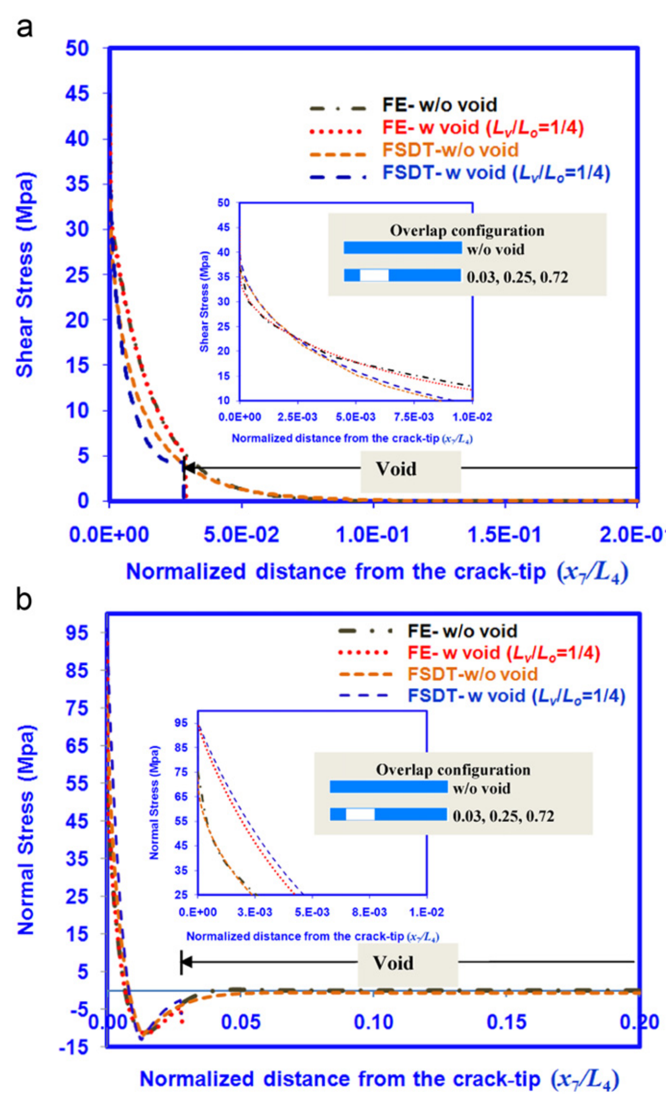

Fig. 8. Comparison of the adhesive (a) shear and (b) normal stress distributions within the overlap area for the single-notch specimen; the inset labeled overlap configuration lists values of L_i/L_o, L_v/L_o, $(L_o-L_i-L_v)/L_o$.

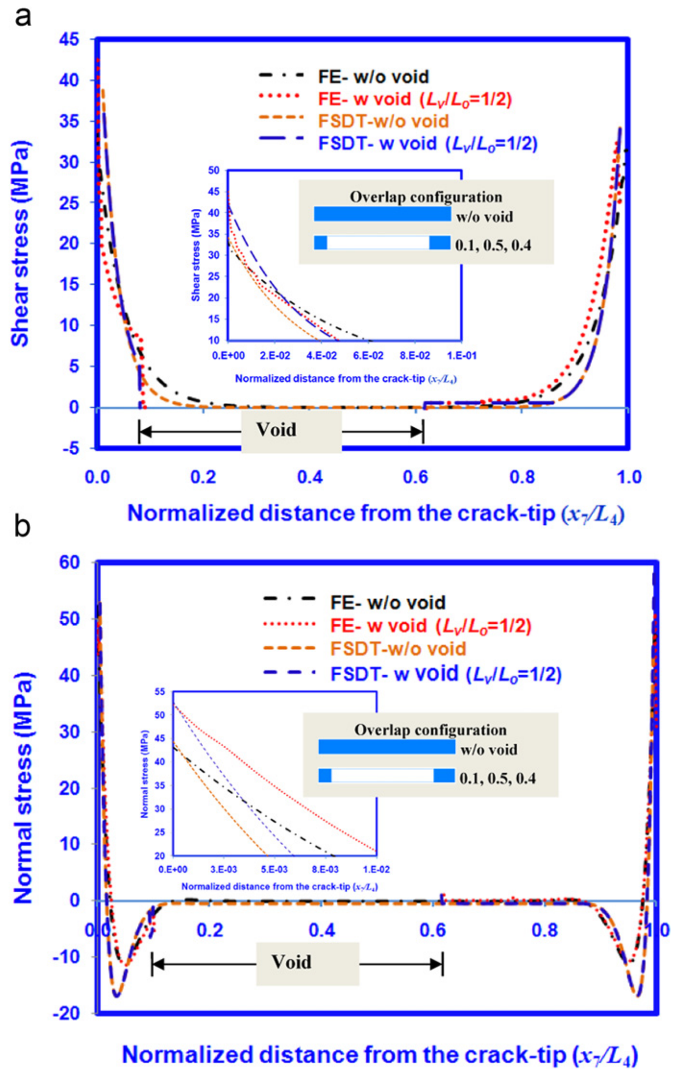

Fig. 9. Comparison of the adhesive (a) shear and (b) normal stress distributions within the overlap area for the double-notch specimen; the inset labeled overlap configuration lists values of L_i/L_o, L_v/L_o, $(L_o-L_i-L_v)/L_o$.

by the two methods equals 8% and 6%, respectively. Hence the FSDT formulation can be used to compute reliable values of stresses and strains for several preliminary designs. Subsequently, for a few selected designs, the accuracy of computed results can be improved by using the FEM and employing an appropriately refined FE mesh. The singularities in the shear and the normal stresses from the FSDT results could not be captured, whereas the corresponding values of the orders of the stress singularity from the solution by the FEM are 0.32 and 0.4, respectively. For the FSDT, stress distributions in the adhesive were computed using Eqs. (5) and (6). The large values of the tensile normal stress near the free edge between the adhesive and the substrate imply that the two will start separating there. We note that the stress singularity at the corner is due to our using the linear elasticity theory. Had we considered material and geometric nonlinearities, we would have obtained finite values of stresses at the edge but the computational cost would have increased considerably. The normal stress at the interface is tensile for $0<x_7/L_4<0.01$.

Results exhibited in Figs. 8 and 9 also reveal that the presence of the void of normalized length $L_v/L_o=1/4$ and $L_v/L_o=1/2$ in single-notch and double-notch specimens, respectively, does not affect much the stress distribution near the free edge of the adhesive/substrate interface. However, at the corners of the free edges of the adhesive adjoining the void and the substrate, the shear stress rapidly drops to zero. The normal stress in the vicinity of the crack tip is tensile; it becomes compressive as one goes away from the crack tip implying that the adhesive and

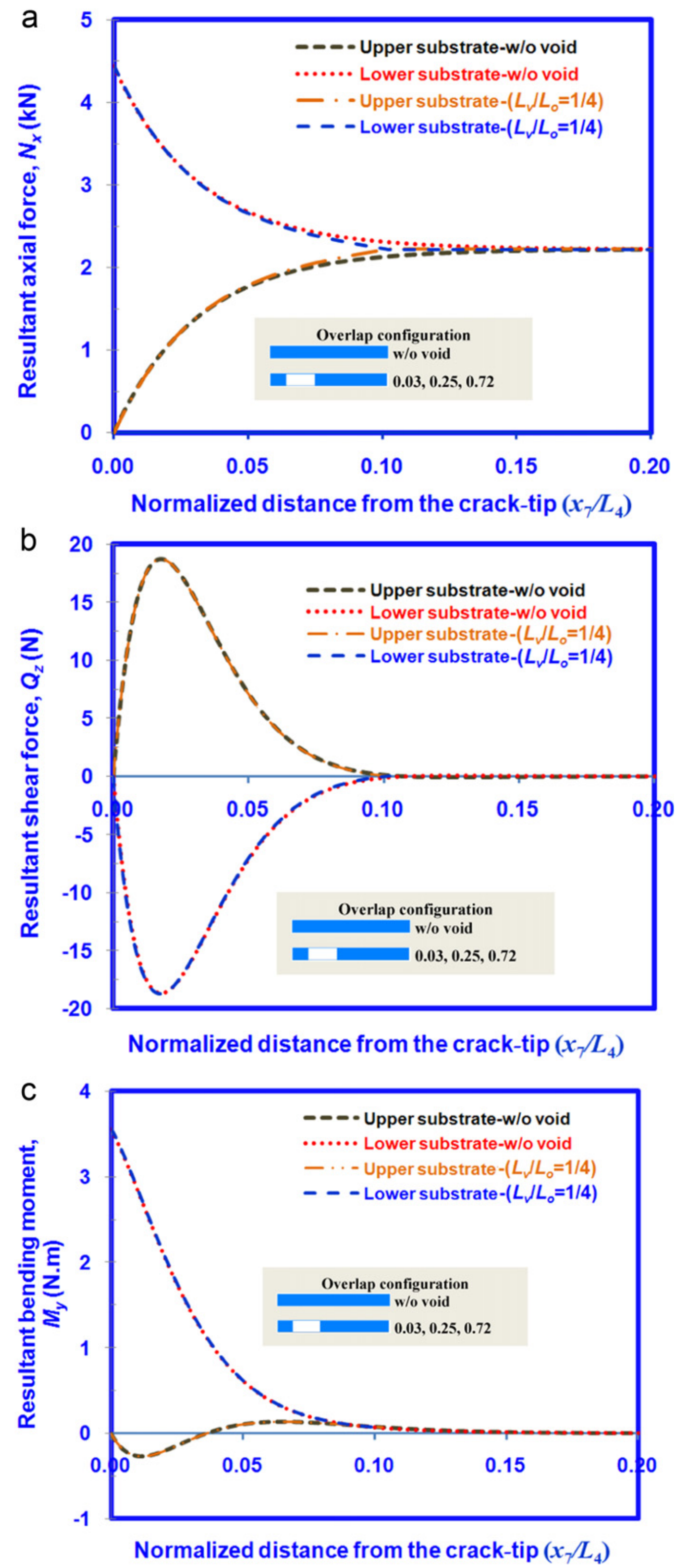

Fig. 10. Comparison of the resultant (a) axial force, (b) shear force, and (c) bending moment for a single-notch specimen (*i*) without void and (*ii*) with void having $L_v/L_o=1/4$; the inset labeled overlap configuration lists values of L_i/L_o, L_v/L_o, $(L_o-L_i-L_v)/L_o$.

the adherend are in contact with each other, and then it gradually goes to zero near the void tip. Unless one uses a very fine mesh, the traction boundary conditions are approximately satisfied in the analysis of the problem by the FEM. Here we have not used a very fine mesh near the void tip resulting in the traction boundary conditions near the void tip being not well satisfied. The plate theory is an idealization of the 3-D elasticity theory and cannot be expected to satisfy point-wise boundary conditions. In order to see how the void affects the resultant axial and shear forces transmitted through the specimen, we have plotted their variations along the x-axis as well as that of the bending moment in Figs. (10a–c) and (11a–c) for the single-notch and the double-notch specimens, respectively. It is clear that the presence of the void does not change the force transmitted through the specimen implying that it does not affect the load carrying capacity of the joint. We note that some of the results exhibited in Figs. 8–11

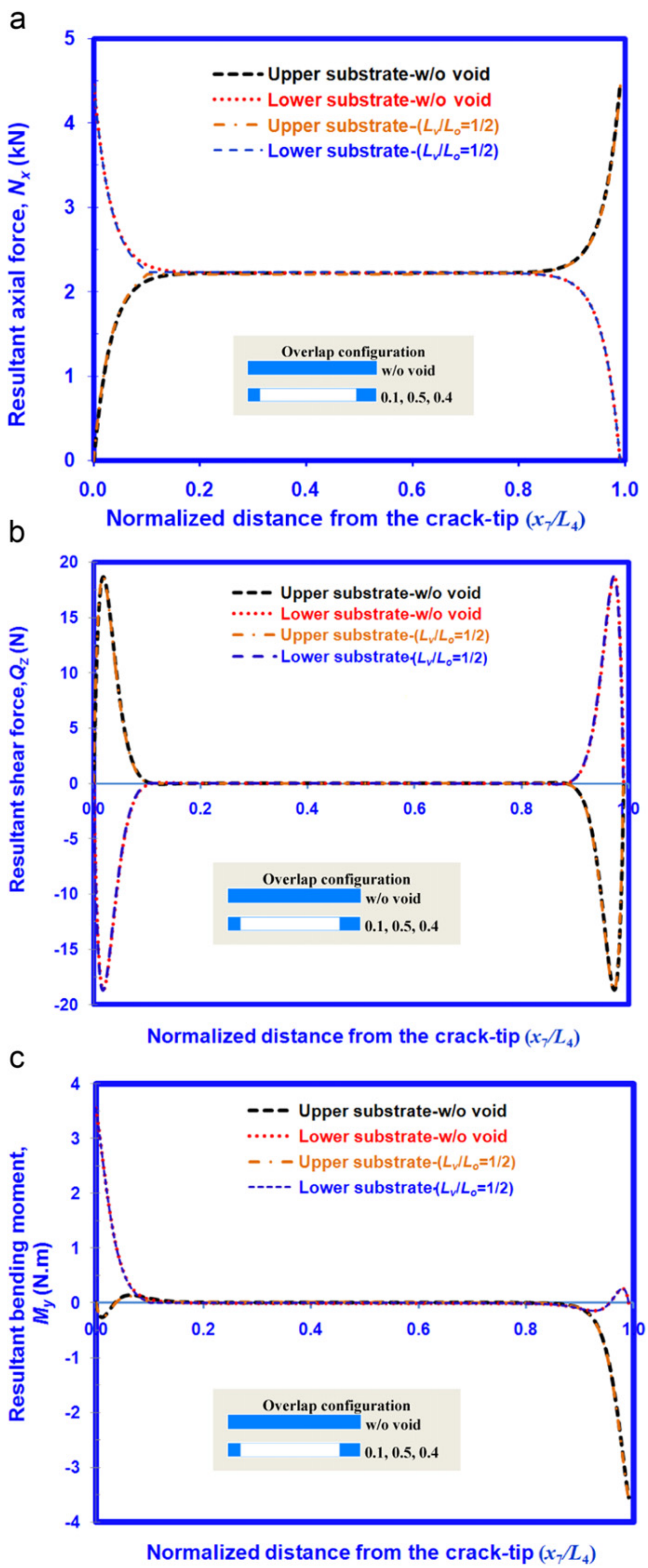

Fig. 11. Comparison of the resultant (a) axial force, (b) shear force, and (c) bending moment for a double-notch specimen (i) without void and (ii) with void having $L_v/L_o=1/2$; the inset labeled overlap configuration lists values of L_i/L_o, L_v/L_o, $(L_o-L_i-L_v)/L_o$.

Table 1
Comparison of crack-tip forces and bending moment.

	FEM	FSDT
Q_c (N)	73.84	71.19
N_c (N)	69.84	67.35
M_c (N mm)	2.22	2.40

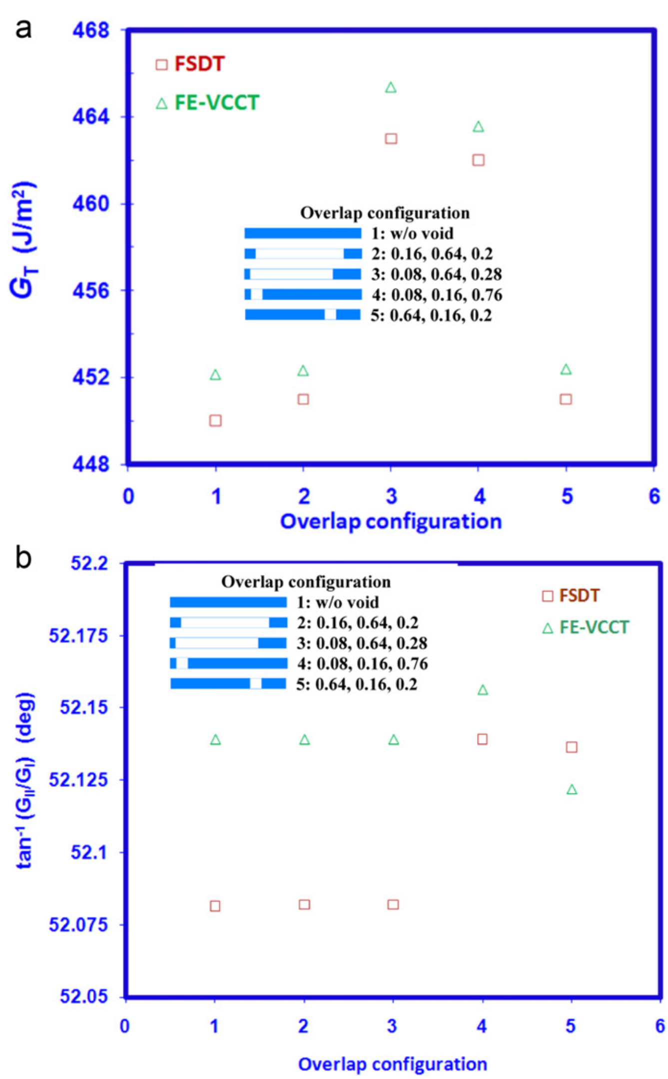

Fig. 12. For single-notch specimen with different void location and length, comparison of (a) total SERR and (b) the mode-mixity parameter computed from results of the FSDT and the FE-VCCT; the inset labeled overlap configuration lists values of L_i/L_o, L_v/L_o, $(L_o-L_i-L_v)/L_o$.

have been obtained by Hart-Smith [10,34] by using a shear lag model. These are included here for the sake of completeness and to show that our approach also gives results close to those derived by Hart-Smith.

For a case with substrate thickness $h^U = h^L = 1.6$ mm, the equivalent crack-tip forces and bending moment found from the results of the FSDT and the FE simulations are compared in Table 1.

For different overlap configurations, we have plotted in Figs. 12 and 13 the total SERR and the mode-mixity parameter computed by using Eqs. (12) and (13). The configurations studied have different values of $(L_i/L_o, L_v/L_o, (L_o - L_i - L_v)/L_o)$, which represent the effect of the void location and its length. We refer the reader to Fig. 1 for definitions of L_o, L_i, and L_v. It is clear that for a given overlap configuration number (horizontal axis) the total SERR (the mode-mixity parameter) computed from the results of the FSDT is about 1% (2.4%) less than that obtained from the solution of the problem by the FEM. Thus the use of the FSDT to analyze the adhesive joint provides very good values of the SERR with a rather modest computational effort as compared to that required for the FEM. Whereas the mode-mixity parameter is essentially the same for all configurations including the one without the void the SERR depends upon the configuration. For the configurations studied, the maximum value of the SERR differs from the minimum value of the SERR by about 3.5% implying that the presence of the void and where it is located does not affect much the load carrying capacity of the joint. However, it is very likely that the presence of a void would have a noticeable effect for a ductile adhesive, which will deform plastically in the overlap region. As also pointed out by Pires et al. [48] using a compliant adhesive diminishes stress concentrations and the joint strength is higher than that for a stiff adhesive.

For different void lengths and locations we have compared in Fig. 14 the effect of the substrate thickness on the total SERR for single- and double-notch specimens. It can be observed that doubling the thickness of the substrate does not change the mode-mixity parameter but reduces the SERR by about 50%. For $h^U = h^L = 3.2$ mm, we have plotted in Fig. 15 the mode-mixity parameter for different overlap lengths. It is clear that the presence of the right notch does not change the mode-mixity parameter but increases the SERR by about 4%.

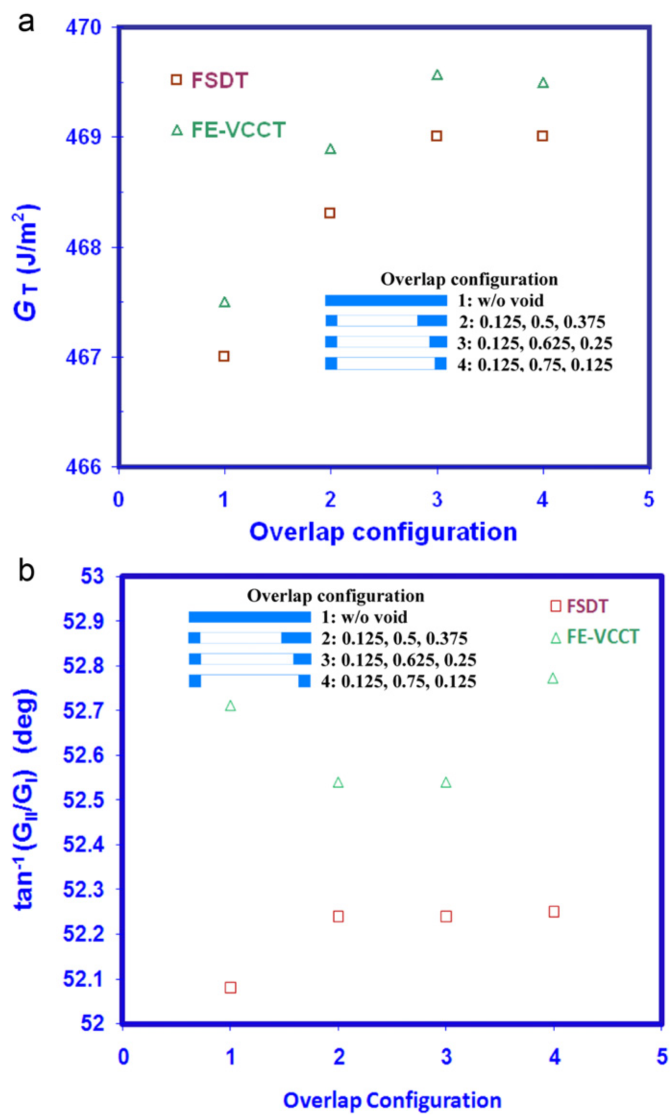

Fig. 13. For double-notch specimen with different void location and length, comparison of (a) total SERR and (b) the mode-mixity parameter computed from results of the FSDT and the FE-VCCT; the inset labeled overlap configuration lists values of L_i/L_o, L_v/L_o, $(L_o - L_i - L_v)/L_o$.

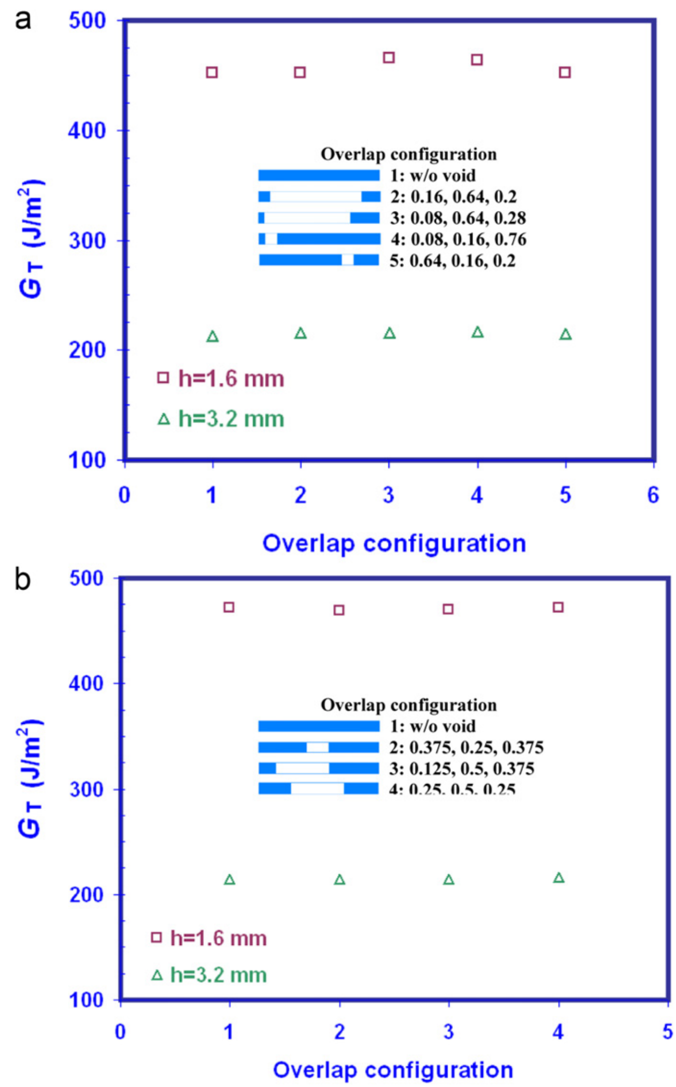

Fig. 14. Effect of substrate thickness on the total SERR for (a) single-notch and (b) double-notch specimens with different void location and size; the inset labeled overlap configuration lists values of L_i/L_o, L_v/L_o, $(L_o - L_i - L_v)/L_o$.

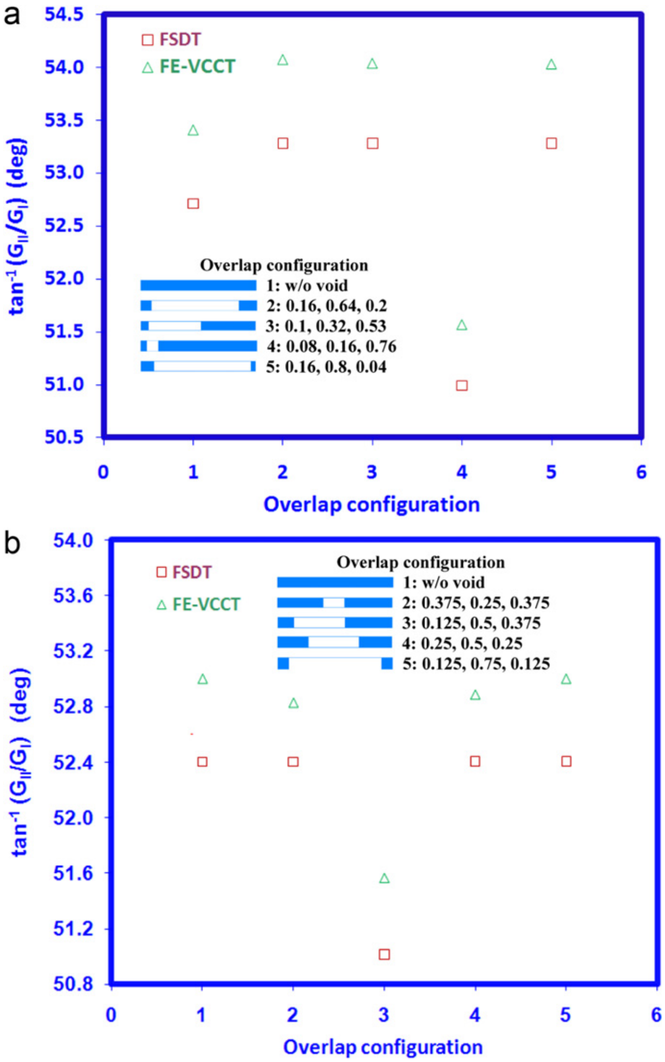

Fig. 15. Comparison of the mode-mixity parameter for (a) single-notch and (b) double-notch with different void location and size; the inset labeled overlap configuration lists values of L_i/L_o, L_v/L_o, $(L_o-L_i-L_v)/L_o$.

6. Conclusions

We have used the first-order shear deformation plate theory (FSDT) to analyze infinitesimal deformations of an adhesive-bonded lap joint specimen conforming to the ASTM D3165 specifications, and have considered the effect of a void. It is found that values of the strain energy release rate (SERR) and the mode-mixity parameter β found from results of the FSDT differ by less than 4% from the corresponding values computed from the solution of the problem by the finite element method. Furthermore, the presence of a void and where it is located have minimal effects on values of the SERR and β.

Thus the FSDT can be used to analyze adhesive-bonded lap joints. The presence of the void of reasonable length does not deteriorate much the load carrying capacity of the joint.

Acknowledgments

This work was partially supported by the Office of Naval Research grant N00014-1-06-0567 to Virginia Polytechnic Institute and State University with Dr. Y. D. S. Rajapakse as the program manager. Views expressed in the paper are those of authors and neither of the funding agency nor of VPI&SU.

References

[1] Andrews EH, Kinloch AJ. Mechanics of adhesive failure I. Proc R Soc Lond A 1973;332:339–85.
[2] Andrews EH, Kinloch AJ. Mechanics of adhesive failure II. Proc. R Soc Lond A 1973;332:401–14.
[3] Adams RD, Peppiatt NA. Stress analysis of adhesively bonded lap joints. J Strain Anal 1974;9:185–96.
[4] Wake WC. Theories of adhesives and uses of adhesives: a review. Polymer 1978;19:291–308.
[5] Adams RD, Comyn J, Wake WC. Structural adhesive joints in engineering. 2nd ed.. London: Chapman and Hall; 1997.
[6] Tomblin JS, Seneviratne W, Escobar P, Yoon-Khian Y. Shear stress–strain data for structural adhesives. Technical Report DOT/FAA/AR-02/97, U.S. Department of Transportation: Office of Aviation Research; 2002.
[7] Dundurs J. Discussion of edge-bonded dissimilar orthogonal elastic wedges under normal and shear loading. J Appl Mech 1969;36:650–2.
[8] Goland M, Reissner E. The stresses in cemented joints. J Appl Mech 1944;11:A17–22.
[9] Erdogan F, Ratwani MM. Stress distribution in bonded joints. J Compos Mater 1971;5:378–93.
[10] Hart-Smith LJ. Adhesive-bonded single-lap joints. Douglas Aircraft Co., Technical Report NASA-CR-1973-112236; 1973.
[11] Kutscha D. Mechanics of adhesive-bonded lap-type joints: survey and review. Technical Report AFML-TDR-64-298, U.S. Air Force Mater. Lab Wright-Patterson AFB; 1964.
[12] Kutscha, D, Hofer Jr. KE. Feasibility of joining advanced composite flight vehicles. Technical Report AFML-TR-68-391, U.S. Air Force; 1969.
[13] Matthews FL, Kilty PF, Goodwin EW. A review of the strength of joints in fiber-reinforced plastics: part 2 adhesively bonded joints. Composites 1980;13:29–37.
[14] Vinson JR. Adhesive bonding of polymer composites. Polym Eng Sci 1989;29:1325–31.
[15] da Silva LFM, das Neves PJC, Adams RD, Spelt JK. Analytical models of adhesively bonded joints—part I: literature survey. Int J Adhes Adhes 2009;29:319–30.
[16] Zhao X, Adams RD, da Silva LFM. A new method for the determination of bending moments in single lap joints. Int J Adhes Adhes 2010;30:63–71.
[17] Tsai MY, Morton J. An evaluation of analytical and numerical solutions to the single-lap joint. Int J Solids Struct 1994;13:2537–63.
[18] Yang C, Pang SS. Stress–strain analysis of single-lap composite joints under tension. J Eng Mater Tech 1996;118:247–55.
[19] Huang H, Yang C, Tomblin JS, Harter P. Stress and failure analyses of adhesive-bonded composite joints using ASTM D 3165 specimens. ASTM J Compos Tech Res 2002;24:345–56.
[20] Yang C, Huang H, Tomblin JS, Sun W. Elastic–plastic model of adhesive-bonded single-lap composite joints. J Compos Mater 2004;38:293–309.
[21] Krueger, D. The virtual crack closure technique: history, approach and applications, Technical Report NASA-CR-2002-211628, ICASE Report no. 2002-10; 2002.
[22] Davidson BD, Yu L, Hu H. Delamination of energy release rate and mode mix in three-dimensional layered structures using plate theory. Int J Fract 2000;105:81–104.
[23] Kim IG, Kong CD. Generalized theoretical analysis method for free-edge delaminations in composites. J Mater Sci 2002;37:1875–80.
[24] Luo. Q, Tong L. Calculation of energy release rates for cohesive and interlaminar delamination based on the classical beam-adhesive model. J Compos Mater 2009;43:331–48.
[25] Yang C, Sun W, Tomblin JS, Smeltzer SS. A semi-analytical method for determining the strain energy release rate of cracks in adhesively-bonded single-lap composite joints. J Compos Mater 2007;41:1579–602.
[26] da Silva LFM, das Neves PJC, Adams RD, Spelt JK. Analytical models of adhesively bonded joints—part II: comparative study. Int J Adhes Adhes 2009;29:331–41.
[27] Wang, JT, Xue DY, Sleight DW, Housner JM. Computation of energy release rate for cracked composite panels with nonlinear deformation. In: Proceedings of the 36th AIAA/ASME/ASCE/AHS/ASC structures, structural dynamics and materials conference, AIAA-95-1463-CP; 1995. p. 2713–27.
[28] Wei Y, Yang T, Wan Z, Du X. New VCCT and its application in composite delamination analysis. China J Comput Mech 2000;17:308–12.
[29] Crocombe AD, Bigwood DA, Richardson G. Analyzing joints for structural adhesive failure. Int J Adhes Adhes 1990;10:167–78.
[30] Fernlund G, Papini M, McCammond D, Spelt JK. Fracture load prediction for adhesive joints. Compos Sci Tech 1994;51:587–600.
[31] Chadegani A, Yang C, Dan-Jumbo E. Strain energy release rate analysis of adhesive-bonded composite joints with a prescribed interlaminar crack. J Aircr 2009;46:203–15.
[32] Chen Z, Adams RD, da Silva LFM. The use of the J-integral vector to analyze adhesive bonds with and without a crack. Int J Adhes Adhes 2011;31:48–55.
[33] Yang C, Chadegani A, Tomblin JS. Strain energy release rate determination of prescribed cracks in adhesively bonded single-lap composite joints with thick bondlines. Compos B: Eng 2008;39:863–73.
[34] Hart-Smith LJ. Further developments in the design and analysis of adhesive-bonded structural joints. In: Keward KT, editor. Joining of composite materials, 749. ASTM STP; 1981. p. 3–31.

[35] Kan HP, Ratwani MM. Stress analysis of stepped-lap joints with bondline flaws. J Aircr 1983;20:848–52.
[36] Rossettos JN, Zang E. On the peak stresses in adhesive joints with voids. J Appl Mech 1993;60:559–60.
[37] Rossettos JN, Lin P, Nayeb-Hashemi H. Comparison of the effects of debonds and voids in adhesive joints. J Eng Mater Tech 1994;116:533–8.
[38] Rossettos JN, Shishesaz M. Stress concentration in fiber composite sheets including matrix extension. J Appl Mech 1987;54:723–4.
[39] Olia M, Rossetos JN. Analysis of adhesively bonded joints with gaps subjected to bending. Int J Solids Struct 1996;33:2681–93.
[40] Lang TP, Mallick PK. The effect of recessing on the stresses in adhesively bonded single-lap joints. Int J Adhes Adhes 1999;19:257–71.
[41] de Moura MFSF, Daniaud R, Magalhaes AG. Simulation of mechanical behaviour of composite bonded joints containing strip defects. Int J Adhes Adhes 2006;26:464–73.
[42] You M, Yan Z, Zheng X, Yu H, Li Z. A numerical and experimental study of gap length on adhesively bonded aluminum double-lap joint. Int J Adhes Adhes 2007;27:696–702.
[43] ASTM D3165-07. standard test method for strength properties of adhesives in shear by tension loading of single-lap-joint laminated assemblies. 2007.
[44] ABAQUS user manual and software, Version 6.9-1, Simulia Dassault Systèmes, Providence, RI; 2009.
[45] Bogy DB, Wang KC. Stress singularities at interface corners in bonded dissimilar isotropic elastic materials. Int J Solid Struct 1971;7:993–1005.
[46] Qian ZQ, Akisanya AR. Wedge corner stress behavior of bonded dissimilar materials. Theor Appl Fract Mech 1999;32:209–22.
[47] Weissberg V, Arcan M. Invariability of singular stress fields in adhesive bonded joints. Int J Fract 1992;56:75–83.
[48] Pires I, Quintino L, Durodola JF, Beevers A. Performance of bi-adhesive bonded aluminum lap-joints. Int J Adhes Adhes 2003;23:215–23.